Hoque *et al. Satellite Navigation* (2025) 6:33
https://doi.org/10.1186/s43020-025-00182-9

Satellite Navigation
https://satellite-navigation.springeropen.com/

ORIGINAL ARTICLE Open Access

Multi-layer ionosphere mapping function for ground and LEO GNSS data and its performance analysis

Mohammed Mainul Hoque[1*], Liangliang Yuan[2], Grzegorz Nykiel[1], Olaf Frauenberger[1], Jacek Paziewski[3], Rafal Sieradzki[3], Pawel Wielgosz[3], Narayan Dhital[4] and Raül Orús Pérez[5]

Abstract

When estimating ionospheric Total Electron Content (TEC) using Global Navigation Satellite System (GNSS) observations, one of the significant error sources is the mapping error introduced by slant to vertical TEC conversion and vice versa. A single-layer Mapping Function (MF) based on a thin-shell assumption of the Earth's ionosphere is commonly used for TEC conversion. However, the accuracy of single-layer MF is susceptible to the inaccurate fixing of the ionospheric single-layer height. In order to find a mapping approach less sensitive to the choice of ionospheric effective height we defined a multi-layer ionosphere mapping function and investigated its performance in comparison with the single-layer model. We found that the multi-layer MF outperforms the single-layer MF when computing GNSS receiver Differential Code Biases (DCBs) especially at low latitude and equatorial regions where ionosphere is highly dynamic and difficult to model. When compared with the International GNSS Services (IGS) products, we found that the mean receiver DCB estimation is improved (closer to benchmark) by about 0.14 – 0.27 ns and 0.30 – 0.78 ns during days in 2019 and 2023, respectively. We found that the receiver DCB estimation improves for about 66–87% receivers. This is also reflected in Global Ionosphere Maps (GIMs) showing better performance for the multi-layer MF when comparing with IGS GIMs. Our investigation using GNSS observations onboard Low Earth Orbiting (LEO) satellites shows that the multi-layer MF can be successfully applied in computing satellite and receiver DCBs accurately.

Keywords GNSS, Ionosphere, Multi-layer mapping function, Differential code biases DCBs, LEO DCBs

Introduction

The dual-frequency Global Navigation Satellite System (GNSS) observations are commonly used to estimate ionospheric Total Electron Content (TEC), and satellite and receiver Differential Code Biases (DCBs). When estimating the GNSS TEC and DCBs in a simultaneous process, one of the significant error sources is the mapping error introduced by the ionosphere Mapping Function (MF) used for slant to vertical TEC conversion and vice versa. A single-layer MF or modified single-layer MF (Schaer et al., 1998) based on a thin-shell assumption of the Earth's ionosphere is commonly used for TEC conversion. The factor that significantly impacts the accuracy of the single-layer MFs is the inaccurate fixing of the ionospheric thin-shell height (Yuan et al., 2021). The single-layer shell-height is often called as the ionospheric effective height. It is assumed that the integrated electron content below and above the effective height is

*Correspondence:
Mohammed Mainul Hoque
Mainul.Hoque@dlr.de
[1] German Aerospace Center (DLR), Neustrelitz, Germany
[2] Shanghai Astronomical Observatory, Chinese Academy of Sciences, Shanghai, China
[3] University of Warmia and Mazury in Olsztyn (UWM), Olsztyn, Poland
[4] DLR Gesellschaft Für Raumfahrtanwendungen mbH (GfR), Weßling, Germany
[5] European Space Agency (ESA), ESTEC, Noordwijk, Netherlands

equal. Therefore, the actual effective height depends on the electron density profile's shape which again varies with varying geophysical and solar conditions.

For simplicity, different GNSS TEC processing centers use fixed values for ionospheric effective height when computing Global Ionosphere Maps (GIMs) using ground data. For example, International GNSS Service (IGS) centers (e.g., Center for Orbit Determination in Europe- CODE, Universitat Politècnica de Catalunya- UPC, Jet Propulsion Laboratory- JPL) use 450 km, Ionosphere Monitoring and Prediction Center (IMPC, Berdermann et al., 2014) of German Aerospace Center (DLR) uses 400 km, and Ground and Space Based Augmentation Systems (GBAS and SBAS) such as the American WAAS (Wide Area Augmentation System) and European EGNOS (European Geostationary Navigation Overlay Service) use 350 km as the ionospheric effective height. However, since the Earth's ionosphere is not spherically symmetric, the effective height varies as functions of geographic location, local time, and solar activity. Considering this, Xiang and Gao (2019) used variable effective heights derived from the International Reference Ionosphere (IRI(Hoque, et al., 2016)) (Bilitza, 2001, see http://irimodel.org/) and found that the mapping errors using variable height are about 8% smaller than those using the fixed height of 450 km. They found the changes in the GNSS satellite DCBs are about 0.1 ns, and larger impacts on the receiver DCBs about 1.0 ns after using variable heights. Recently Huo et al. (2024) proposed a TEC mapping function taking into account not only the receiver-to-satellite elevation angle but also the azimuth angle that reflects the anisotropic variation characteristics of the ionospheric. They obtained a significant reduction in the mapping error compared to the modified single-layer MF.

Again, when estimating the GNSS satellite and receiver DCBs, as well as the corresponding topside ionospheric TEC using onboard Low Earth Orbiting (LEO) satellites observations, the same MF used for the ground data is not applicable. This is due to the change in ionospheric effective height resulting from the different observation height. The higher the LEO height the less the ionospheric contribution above the orbit and the higher would be the effective height.

For LEO based observation, either a thin-layer (or cosine MF) or F&K (Foelsche & Kirchengast, 2002) MF based on a single-layer assumption of the ionosphere is commonly used (see Xiang & Gao, 2019; Zhong et al., 2016). Zhong et al. (2016) evaluated three different MFs, namely Lear MF (Lear, 1988), cosine MF and F&K MF by analyzing their performance in different mapping scenarios. They found that the F&K mapping function together with the effective height from the centroid method (Wang, 2003) is more suitable for the LEO-based TEC conversion. Therefore, like in ground data, the mapping function plays a significant role in LEO topside TEC modelling, and receiver and satellite DCB estimation, and the factor that significantly impacts the accuracy in the single-layer MF is the ionospheric effective height. Considering this, Hoque and Jakowski (2013) and Hoque et al. (2014) proposed a multi-layer mapping approach which is less sensitive to the choice of ionospheric effective height. They assume that the ionosphere is composed of numerous thin shells in between of which the vertical structure is modelled by a Chapman profile. A slant path intersects each ionospheric shell and the intersection points are projected on the thin-shell surface (at 350/400/450 km height) where corresponding vertical delays or TECs are computed. Thus, the slant TEC is computed utilizing the vertical TEC value not only at a single Ionospheric Pierce Point (IPP) rather at many IPPs along the ray path. Although Hoque et al. (2014) applied a single-layer MF in computing the GPS (Global Positioning System) satellite and receiver DCBs, and GIMs using data from a network of ground GNSS stations worldwide, they found that the use of multi-layer MF in computing slant TECs from GIMs reduces the mean errors up to about 50% at low elevation angles ($< 30°$) under high solar activity conditions.

Later, the multi-layer mapping approach is improved by superposing an exponential decay function for describing the topside-ionosphere and plasmasphere in addition to the Chapman function. Yuan et al., (2020, 2021) successfully applied the improved multi-layer MF approach to estimate the GPS satellite and LEO receiver DCBs by combining data from different LEO missions orbiting at different heights. The performance of the multilayer MF is evaluated through model simulations using the IRI (Blitza, 2001) and Global Core Plasmasphere Model (GCPM, Gallagher et al., 2000) and compared with the single-layer MF. The results show that the multilayer mapping function outperforms the F&K mapping function. Yuan et al. (2021) found that the multi-layer MF can successfully reduce the TEC errors resulting from horizontal electron gradient and uncertainties of effective ionospheric heights.

In the current work, for the first time, we have investigated the benefit of using multi-layer MF in computing GPS satellite and receiver DCBs and GIMs using ground data during quiet and perturbed ionospheric conditions. Furthermore, the multi-layer MF approach is applied to onboard LEO satellites data together with a height normalization procedure. The satellite DCBs are subsequently computed and compared with ground-only data.

Multi-layer ionosphere mapping function

In the multi-layer approach, the ionosphere is composed of numerous thin shells in between of which the vertical structure is modelled by a Chapman profile (Chapman, 1931; Rishbeth & Garriott, 1969) and a superposed exponential decay function (Jakowski, 2005) for describing the topside-ionosphere and plasmasphere. Thus, the total ionospheric and plasmaspheric electron density $N_e(h)$ is modeled as a function of height h by

$$N_e(h) = N_m exp\left(\frac{1}{2}(1 - z - exp(-z))\right) + n_p exp\left(-\frac{h}{H_p}\right) \quad (1)$$

where N_m is the peak electron density observed at the altitude h_m, $z = (h - h_m)/H$ and H is the atmospheric scale height. The quantity n_p is the plasmaspheric basic density of electrons and H_p is the mean scale height of the plasma density. We can assume $H = 70$ km which is a moderate value for Chapman layer scale height. The plasmaspheric basic density n_p can be obtained by N_m/k where $k >= 100$ in general (Hoque et al., 2023). The plasmaspheric scale height H_p is much higher than the Chapman layer scale height and can reach up to 10,000 km and can be computed by using an empirical plasmasphere model such as Neustrelitz Plasmasphere Model (NPSM, Jakowski & Hoque, 2018). The multi-layer MF is defined by

$$MF_{multilayer} = \frac{STEC_{model}}{VTEC_{model}} \quad (2)$$

where $STEC_{model}$ is the slant TEC along the ground-to-GNSS (or LEO-GNSS) path and $VTEC_{model}$ is the corresponding vertical TEC (VTEC). The VTEC is defined as the VTEC from the ground (or LEO orbit height) up to GNSS orbit height for which the measurement point is considered at the intersection point between the slant path and the efective height layer (see h_{eff} in Fig. 1). Since the ionosphere is considered to be composed of numerous thin shells, a slant signal path intersects each ionospheric shell characterized by shell heights of $h_1 \ldots h_n$ (see Fig. 1 for illustration). The top and bottom schemes illustrate the ground-GNSS and LEO-GNSS cases, respectively. The intersection points are projected onto a 2D thin-shell surface (red bold arc in Fig. 1), which in case of IGS GIM is at 450 km (Schaer et al., 1998), where corresponding VTECs are computed from a TEC map or GIM (alternatively by any 2D TEC model) as $VTEC_{IPP1}$, $VTEC_{IPP2}$ … $VTEC_{IPPi, \ldots}$ etc. Thus, $STEC_{model}$ can be calculated from incremental STEC namely $\Delta STEC_1$, $\Delta STEC_2$ … $\Delta STEC_i$ by

$$\begin{aligned} STEC_{model} =& \Delta STEC_1 + \Delta STEC_1 + \Delta STEC_i + \ldots = f(VTEC_{IPP1})l_1 \\ &+ f(VTEC_{IPP2})l_2 + \ldots + f(VTEC_{IPPi})l_i + \ldots \\ &= Ne_1 l_1 + Ne_2 l_2 + Ne_i l_i + \ldots \end{aligned} \quad (3)$$

where $f(VTEC)$ denotes a function of VTEC. Similarly we can write.

$$\begin{aligned} VTEC_{model} =& f(VTEC_{IPPi})(h_2 - h_1 \\ &+ h_3 - h_2 + \ldots h_i - h_{i-1} + \ldots) \\ &= Ne_1 \Delta h_1 + Ne_2 \Delta h_2 + \ldots + Ne_i \Delta h_i + \ldots \end{aligned} \quad (4)$$

Equation (3) indicates that $\Delta STEC_1$, $\Delta STEC_2$ … $\Delta STEC_i$ can be computed along the ray path multiplying the corresponding electron densities Ne_1, Ne_2 … Ne_i by the length of each segment (l_1, l_2, … see plots of Fig. 1). Equation (1) indicates that the electron densities can be derived if Chapman layer parameters such as the peak ionization N_{m1}, N_{m2}, … N_{mi}, peak height h_{m1}, h_{m2}, … h_{mi}, atmospheric scale height H_1, H_2, … H_i and plasmaspheric basic densities n_{p1}, n_{p2}, … n_{pi} are known. The Chapman layer approximation $VTEC = 4.13 HN_m$ (Hoque & Jakowski, 2007) can be used for computing N_{mi} using $VTEC_{IPPi}$ for fixed $H_i = 70$ km. The h_{mi} (= 350 km) and H_i (= 70 km) can be kept constant for simplicity, alternatively empirical model (e.g., Neustrelitz Peak Height Model- NPHM, Neustrelitz Equivalent Slab Thickness Model- NSTM by Hoque and Jakowski, (2012), and Jakowski and Hoque, (2021), respectively) values can be used.

The plasmaspheric basic density n_{pi} can be determined dividing N_{mi} by a predefined factor as mentioned earlier. Finally, $STEC_{model}$ (black bold line in Fig. 1) is computed by summing all the $\Delta STEC$ values. Similarly, $VTEC_{model}$ (blue broken line) is computed by summing all the $\Delta VTEC$ values. The reference location of the VTEC is identified as the intersection point of the slant path and the effective height layer. Thus, when both $STEC_{model}$ and $VTEC_{model}$ are computed, finally $MF_{multi\text{-}layer}$ is computed by Eq. (2). The proposed approach avoids using any 3D electron density model rather uses TEC maps from 2D model or external sources (e.g., IGS GIMs).

The multi-layer MF is capable of considering the ionospheric horizontal electron gradient effects by making use of the background VTEC map. The introduction of ionospheric electron density profiles is found to be beneficial to reduce the effects of uncertainties of effective ionospheric heights. Thus, an apparent advantage of the multi-layer MF is that the performance of the

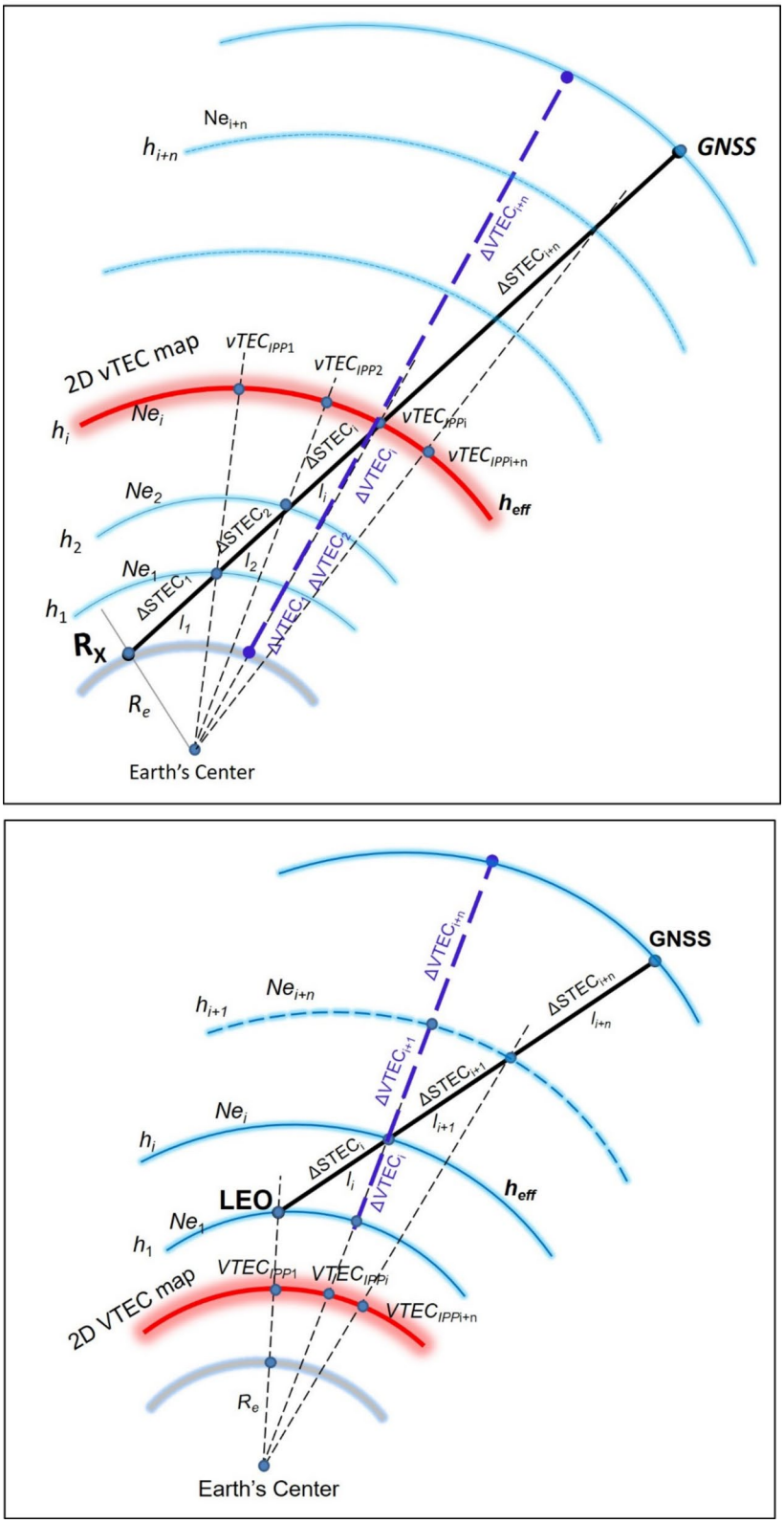

Fig. 1 Schematics of multi-layer MF for the ground and LEO based data. The symbols R_X, LEO and GNSS correspond to the location of the ground and LEO receivers, and GNSS satellite, respectively, and R_e is the Earth's radius

multi-layer MF does not strongly depend on the choice of the effective ionospheric height while the change of effective height will result in a VTEC conversion bias in single-layer mapping functions. It is noted that the multi-layer MF still requires an approximate effective height for locating measurement points; however, its influence is limited. In the present case we consider effective height as the receiver height plus 450 km regardless of ground or LEO data.

Combining data from multiple LEO satellites

The topside TEC measurements onboard LEO satellites contain non-equivalent vertical TEC information due to significantly different LEO orbit heights (in present case orbit height varies from 450 to 800 km). In order to assist the LEO DCB estimation, a vertical TEC model for the topside ionosphere/plasmasphere region between 800 and 20,000 km altitude is parameterized. Note that the lower boundary defines the reference orbit height and the upper boundary represents the approximate height of GNSS satellites. The GNSS topside TEC observations from available LEO missions are combined after normalizing the observations for 800 km reference orbit height (see also Yuan et al., 2021). In fact, a better spatial–temporal coverage will be obtained by combining multi-mission observations. For illustration, in Fig. 2, we considered observations from two satellites namely Swarm-A (LEO_{SW}) and COSMIC-1 (LEO_{CM}) with orbit height of about 460 km and 800 km, respectively.

The ionospheric effective height is considered as the receiver height plus 450 km which defines the measurement location for LEO vertical TECs. Therefore, the effective height will be about 910 km for the receiver onboard Swarm-A satellite and about 1,250 km for the receiver onboard COSMIC-1 satellite. The intersection points between the effective height (labelled as $heff_{SW}$ and $heff_{CM}$ for Swarm-A and COSMIC-1, respectively) circles and the slant signal path define the measurement location for the corresponding LEO vertical TECs. The reference orbit height at $h_{ref}=800$ km is shown by a purple colored arc. The green and black solid lines represent the STEC for COSMIC-1 and Swarm-A links whereas the green and black brocken lines represent the corresponding VTEC for COSMIC-1 and Swarm-A links, respectively. In case of COSMIC-1, the orbit height is the same as the reference height, therefore, the observed $VTEC_{obs\text{-}CM}$ and the reference/normalized $VTEC_{obs\text{-}norm}$ are the same, whereas for Swarm-A the observed $VTEC_{obs\text{-}SW}$ is greater than the reference/normalized $VTEC_{obs\text{-}norm}$ (see Fig. 2). Considering this, for LEOs flying at orbit height lower/higher than the reference height, the observed $VTEC_{obs}$ is reduced/increased multiplying by a factor derived from multi-layer ionosphere model. Applying the multi-layer model, the expressions for $VTEC_{obs}$ and $VTEC_{obs\text{-}norm}$ can be written as

$$VTEC_{obs} = STEC_{obs}.\frac{VTEC_{model}^{h_{LEO}-h_{GNSS}}}{STEC_{model}} \tag{5}$$

$$VTEC_{obs-norm} = VTEC_{obs} \cdot \frac{VTEC_{model}^{h_{ref}-h_{GNSS}}}{VTEC_{model}^{h_{LEO}-h_{GNSS}}} \tag{6}$$

By substituting Eq. (5) in Eq. (6) we can write

$$VTEC_{obs-norm} = STEC_{obs} \cdot \frac{VTEC_{model}^{h_{LEO}-h_{GNSS}}}{STEC_{model}} \cdot \frac{VTEC_{model}^{h_{ref}-h_{GPS}}}{VTEC_{model}^{h_{LEO}-h_{GNSS}}} = STEC_{obs}\frac{VTEC_{model}^{h_{ref}-h_{GPS}}}{STEC_{model}} \tag{7}$$

Where $STEC_{obs}$ is the link-related slant observation, $VTEC_{obs}$ is the corresponding vertical TEC observation between the LEO and GNSS height at the measurement location, $VTEC_{obs-norm}$ is the vertical TEC observation between the reference height and GNSS height, $VTEC_{model}^{h_{ref}-h_{GNSS}}$ is the model vertical TEC between the reference height and GNSS height, and $VTEC_{model}^{h_{LEO}-h_{GNSS}}$ is the model vertical TEC between the LEO and GNSS height. Finally, the multi-layer ionosphere approach is applied to compute the $STEC_{model}$ and $VTEC_{model}^{h_{ref}-h_{GNSS}}$ separately by integrating TEC segments along the slant and vertical ray paths.

Implementation of multi-layer MF

In previous section, we described the multilayer MF approach in details and possibilities of using ionosphere parameters models for providing required vertical structure and spatial gradients information. We implemented the multi-layer MF approach in three different modes based on the use of additional input data and models. In each mode, the background electron density model is composed of a Chapman layer with a superposed exponential decay function describing the ionosphere and plasmasphere. The spherical layers are implemented in such a way that the distance between layers varies depending on the elevation angle of the signal or ray-path. In the current analysis, the slant distance between two consecutive layers is set 50 km in the ionosphere (< 2,000 km altitude) and 200 km in the plasmasphere (> 2,000 km altitude). We defined

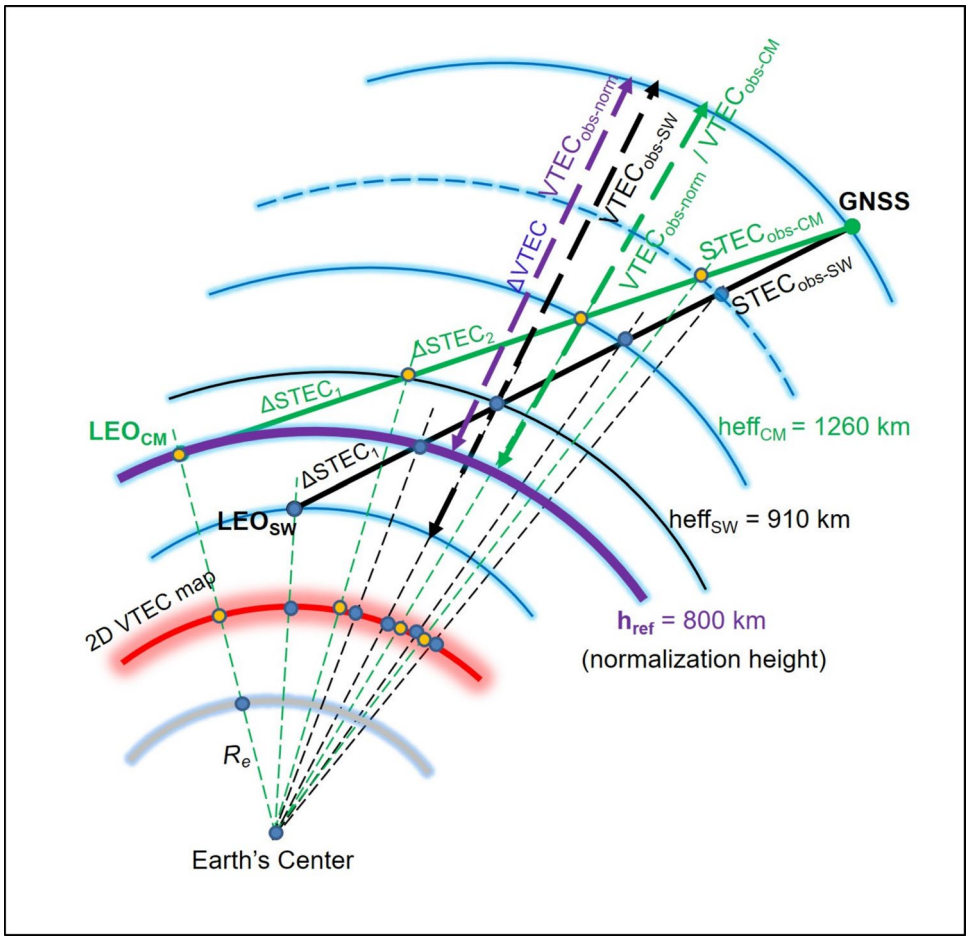

Fig. 2 A schematic illustration of the normalization procedure

the ionospheric effective height as the receiver height plus 450 km regardless of ground or space data. Therefore, the effective height is about 450 km for a ground receiver and it is about 850 km for a LEO receiver orbiting at about 400 km height.

(i) Blind or stand-alone mode

In blind mode, the Chapman layer parameters such as the atmospheric scale height H and peak electron density height h_m are kept constant as 70 km and 350 km, respectively. The VTEC at numerous intersection points along the receiver-satellite link are derived from the Neustrelitz TEC Model (NTCM, Jakowski et al., 2011a) driven by predefined F10.7 value (e.g., 100 solar flux units or sfu, 1sfu = 10^{-22} WHz^{-1} m^{-2}). The corresponding peak density N_m is derived by $N_m = \text{VTEC}/4.13H$ where atmospheric scale height $H = 70$ km. The scale height H_p for exponential decay function is kept fixed as 10,000 km. The plasmaspheric basic density is derived by $n_p = N_m/100$.

(ii) Semi-assisted mode

In semi-assisted mode, the Chapman layer parameters N_m, h_m and corresponding VTECs are computed by NPDM (Neustrelitz Peak Density Model, Hoque & Jakowski, 2011), NPHM and NTCM models. The parameters are derived at numerous intersection points along the receiver-satellite link by driving the models with the actual F10.7 value. The Chapman layer scale height H is computed from the relation $H = \text{VTEC}/4.13N_m$ (Hoque & Jakowski, 2007). The scale height for exponential decay function is computed by NPSM (Jakowski & Hoque, 2018) model. The plasmaspheric basic density is derived by $n_p = N_m/100$.

(iii) assisted or augmented mode

In assisted (or augmented) mode, all parameters except the VTEC are computed like the semi-

assisted mode. The VTECs at numerous pierce points along the receiver-satellite link (after projecting to a 2-D plane at 450 km height) are derived from actual GIMs (e.g., IGS GIMs).

For simplicity, in the current work, we investigated the performance of the blind or stand-alone MF mode in comparison with the single-layer MF. The following Single-Layer Model (SLM) is considered.

$$SLM = \frac{1}{\sqrt{1 - \left(\frac{R_e}{R_e + h_{Ieff}}.cos(ele)\right)^2}} \quad (8)$$

where *ele* is the receiver-to-transmitter elevation angle, R_e=6,371 km is the Earth's mean radius and h_{Ieff}=450 km is the ionospheric effective height.

Three modes of multi-layer MF are defined considering future needs although we could only investigate the performance of the blind or stand-alone mode. We chose the bind mode for its simplicity and tested its performance for DCB estimation and TEC reconstruction. As already mentioned, in Hoque et al. (2014), the multi-layer MF (blind option) was applied to convert vertical TECs to slant TECs from GIMs at test stations although the GIMs were generated using single-layer MF combining data from numerous ground GNSS stations. So, there is a possibility that the user can use any of the three modes for converting VTEC to STEC from GIMs. It is expected that the use of additional information about key ionospheric parameters and actual GIMs instead of NTCM model in the multi-layer MF will improve the performance.

Database and data processing

In order to investigate the performance of the multi-layer MF in comparison with SLM MF, we considered four representative test cases characterized by geomagnetic and solar conditions:

- Test Case #1: Quiet-geomagnetic and low solar activity and winter (summer) condition in the Northern (Southern) hemisphere: selected days 9–10 January 2019
- Test Case #2: Quiet-geomagnetic and low solar activity and summer (winter) condition in the Northern (Southern) hemisphere: selected days 14–15 July 2019
- Test Case #3: Perturbed geomagnetic and high solar activity conditions: selected days 4 and 15 January 2023
- Test Case #4: Quiet-geomagnetic and high solar activity conditions: selected days 9–10 July 2023

Ground data processing

For the above Test cases/days, we collected GNSS dual-frequency code pseudo-range and carrier-phase measurements in terms of daily RINEX (Receiver Independent Exchange Format) files from globally distributed more than 200 ground stations from the NASA's CDDIS (The Crustal Dynamics Data Information System) archived at https://cddis.nasa.gov/archive/gnss/data/daily. The slant TECs are derived by combining both the dual-frequency carrier-phase and code-pseudorange measurements. We used GPS L1 & L2 signals for carrier phases and GPS P1 & P2 signals for code pseudoranges. On one hand, the phase derived TEC is precise and smooth but biased by an unknown phase ambiguity constant. On the other hand, the code derived TEC is not ambiguous but noisy and less precise. The carrier-phase derived TECs are levelled to the code-derived TECs to remove the unknown carrier-phase ambiguities. However, the differential code measurements suffer from the receiver and satellite inter-frequency biases (e.g., DCBs). The multi-layer mapping function (blind option) is now applied to convert the STECs (elevation cut-off 10 degree) to the VTECs at IPP height of about 450 km. It is noted that a fixed IPP height is used to geo-locate the measurements so that one VTEC model can be constructed. The VTECs are fitted to a 15th order spherical harmonic ionosphere model for computing the satellite and receiver DCBs (in our case P1-P2 combination) as well as TECs on daily basis in a simultaneous process.

For details about the TEC calibration and separation of inter-frequency satellite and receiver biases we refer to Jakowski et al. (2011b). We generated GIMs by assimilating TEC observations into the background ionosphere model (i.e., spherical harmonic coefficients) obtained during the bias estimation. A similar procedure described in Jakowski et al. (2011b) is used for TEC assimilation.

For comparison purposes, the whole DCB estimation, TEC calibration and GIM generation process is repeated using SLM MF. The same IGS ground receiver network is used for both cases. This gives us a unique chance of comparing the performance of multi-layer (blind option) and SLM MF with independent data. The GIM products are generated in IONosphere Map EXchange (IONEX) format with 30-min interval, and 2.5-degree latitude and 5-degree longitude resolution.

LEO data processing

For the selected days we collected LEO topside GNSS dual-frequency (code pseudo-range and carrier phases) observations from the following satellite missions: COSMIC-1 (1 satellite, only 2019), COSMIC-2 (6 satellites, only 2023), MetOp (MetOp-A, MetOp-B, MetOp-C),

Swarm (Swarm-A, Swarm-B, Swarm-C), TerraSAR-X and Sentinel (Sentinel-3A, Sentinel-3B). The COSMIC-1, COSMIC-2, MetOp and TerraSAR-X data are collected from UCAR's (University Corporation for Atmospheric Research) COSMIC Data Analysis and Archive Center (CDDAC) archive at https://cdaac-www.cosmic.ucar.edu/. The Swarm data are obtained from the ESA's (European Space Agency) Swarm archived at http://swarm-diss.eo.esa.int or ftp server at ftp://swarm-diss.eo.esa.int/. The Sentinel data are collected from the CDDIS archive at https://cddis.gsfc.nasa.gov/archive/doris/data.

Like ground data, we used GPS L1 & L2 signals for carrier phases, and GPS P1 & P2 signals for code pseudoranges, and the carrier-phase derived TECs are levelled to the code-derived TECs to remove the unknown carrier-phase ambiguities. The multi-layer mapping function (blind option) is applied to convert the STECs (elevation cut-off 10 degree) to the VTECs at IPP height of about 450 km above the LEO receiver height. It is noted that a fixed IPP height is used to geo-locate the measurements so that one VTEC model can be constructed after applying the height normalization for a common height of 800 km. Figure 2 shows a sketch how LEO STEC is projected to VTEC (above LEO height up to GNSS height) at effective ionospheric height (LEO height + 450 km) using a multi-layer MF approach. Since multi-mission LEO data with different orbit height (e.g., 450 km, 550 km, 800 km etc.) are combined, a VTEC normalization method as described in section-2 is used. The normalized VTEC observations are fitted to a 15th order spherical harmonic ionospheric model for estimating GPS satellite and LEO receiver DCBs (in our case P1-P2 combination) as well as topside TECs on daily basis in a simultaneous process.

Reference data or benchmark

As benchmark or reference datasets, the GPS satellite and receiver DCBs and GIMs provided by CODE as the final products (see https://igs.org/products/) are downloaded from the CDDIS archive at https://cddis.nasa.gov/archive/gnss/products/ionex/. The obtained IONEX file contains GPS satellite DCBs for the C1W-C2W combination and receiver DCBs for the C1W-C2W and C1C-C2W combinations. The IGS observation files are commonly provided in RINEX v2.x format and they contain GPS pseudoranges C1, P1 and P2, and therefore, we computed the GPS satellite and receiver DCBs for the P1-P2 combination. When the observation files are mapped into RINEX v3.x format, the GPS C1, P1 and P2 signals are mapped to C1C, C1W and C2W observation codes, respectively (Wang et al., 2020). Considering this, we compared our P1-P2 DCBs with the C1W-C2W DCBs provided by CODE. Therefore, whenever we mention satellite and receiver DCBs we mean corresponding P1-P2 DCBs hereafter. As a second benchmark, we downloaded IGS combined GIM and DCB products from the CDDIS archive. The combined IGS final products are generated by combining GIM products from a number of IGS associate centers (e.g., CODE, UPC, ESA, Jet Propulsion Laboratory-JPL, Chinese Academy of Sciences-CAS, etc.). Note that the combined IONEX file does not include any information regarding the signal combination (i.e., P1-P2 or C1W-C2W or C1C-C2W) used in the satellite and receiver DCB estimation and GIM generation. For comparison purpose, we assume that the same signal combination (i.e., P1-P2 or C1W-C2W) is used for LMAP (LEO ionospheric Mapping Assessment and derivation for Precise PVT Applications) and combined IGS products which may not be true for all satellites and receivers.

The Jason-3 vertical TEC data are collected from Open Altimeter Database at https://openadb.dgfi.tum.de/en/missions/jason3/107/. Jason-3 provides vertical TECs below the orbit height (~1,330 km) mainly over the oceans. The altimeter measurements are naturally vertical and therefore, no mapping function is required. The reference/legacy LEO receiver DCBs are obtained from the UCAR's CDDAC and ESA's Swarm archives already mentioned.

Performance analysis of multi-layer MF

The execution of Test Cases provided ionospheric data products such as the GPS satellite and receiver (LEO, ground) DCBs, absolute/calibrated TECs and vertical TEC maps in terms of GIMs. The investigation is conducted within the scope of an ESA supported project called LMAP and therefore the generated products are named as LMAP products hereafter. In the following the ionospheric products are validated by.

- comparing obtained GPS satellite and LEO receiver DCBs against reference/legacy DCBs from IGS, UCAR and ESA sources.
- comparing obtained GNSS satellite and ground receiver DCBs against reference/legacy DCBs from IGS sources (e.g., CODE).
- computing and comparing modelled vertical TEC from ground data against IGS/CODE GIMs.
- computing and comparing modelled vertical TEC against Jason-3 altimeter data.

In case of ground data, the ionospheric products are generated using multi-layer MF and single-layer MF separately. Both types of data products were compared with independent similar reference data products.

GPS satellite and receiver DCBs

In this section, the GPS satellite and receiver (LEO, ground) DCBs are compared against CODE and IGS data products. The comparison is done for each test cases separately. We obtained very similar results when comparing LMAP products with CODE and IGS data products. The used signal combinations for DCBs are known for CODE products and therefore we provided relevant plots for comparison with CODE products (see Figs. 3 and 4). However, the discussion includes results from both comparisons. As an exception, Fig. 5 includes plots for comparison with both CODE and IGS products. The blue bars in left panel of Fig. 3 show the GPS satellite DCBs provided by CODE. The green and red bars show GPS satellite DCBs computed using multi-layer (blind option) and single-layer MF, respectively, in current analysis. The green (multi-layer MF) and red bars in right panel show the differences between the CODE and computed satellite DCBs in current analysis.

Figure 3 shows that most cases the satellite DCBs differ within ± 1 ns when compared with CODE DCB product during low solar activity days in 2019. However, the differences are increased up to 2 ns during high solar activity days in 2023. We found that both LMAP products (multi-layer MF and single-layer MF) give similar difference plots in right panel, and there is hardly any influence of MF choice in satellite DCB estimation from ground data. The comparison with IGS satellite DCBs gives similar deviations of ± 1 and ± 2 ns during selected low and high solar activity, respectively. The differences from the CODE DCBs during quiet as well as disturbed conditions can be explained by the use of different methods and/or GNSS stations. As for example, CODE's DCB estimation involves processing of GNSS data from a network of stations over the 3-day period whereas we used daily data.

Figure 4 compares the GPS ground receiver DCBs between CODE product and our estimation. The green (multi-layer-MF, blind option) and red (single-layer-MF) bars show the differences (DCB_{LMAP} minus DCB_{CODE}) between the CODE product and our computation for selected days in 2019 and 2023. The number in x-axis denotes individual receivers.

Comparing the top and bottom plots in Fig. 4, we find that the receiver DCB differences between the CODE product and our computation are increased by about 2 ns during perturbed and high solar activity days. The same is true when comparing with IGS combined products. Ionosphere is more dynamic during high solar activity conditions and difficult to model; therefore, we obtained higher modelling errors for mapping function regardless of the choice of the mapping function. We see that the green bars (multi-layer-MF) are closer to the zero-difference line indicating a better performance (i.e., closer to the benchmark) for the multi-layer MF option compared to the single-layer MF. When compared with CODE DCBs, we found that the mean receiver DCB estimation is improved by about 0.14 – 0.25 and 0.32 – 0.78 ns during days in 2019 and 2023, respectively, after using multi-layer MF instead of the single-layer MF. The values are 0.14 – 0.27 ns and 0.30 – 0.70 ns, respectively, when comparing with IGS DCBs.

The maximum improvement (i.e., closer to the benchmark) is found to be 0.75 and 2.2 ns during 2019 and 2023, respectively, for both CODE and IGS cases. We found that the receiver DCB estimation improves (i.e., closer to CODE Benchmark) for about 68–81% and 68–87% receivers/stations during 2019 and 2023, respectively. When considering IGS DCBs as the benchmark, the improvements (i.e., closer to IGS benchmark) are found for about 68–79% and 66–82% receivers/stations during 2019 and 2023, respectively. Noted that our computation mostly underestimates (see -ve deviation) the ground receiver DCBs when comparing with the CODE/IGS product. Again, for a few cases the green error bar is larger than the red bar indicating larger error for the multi-layer MF (see bars with + ve sign indicating over estimation). The geolocation of those receivers is shown in Fig. 6 and possible reason of such large errors is discussed.

Although a similar station network is used, Figs. 3 and 4 show that there are differences between the CODE and our DCB computation. The GNSS satellite and receiver DCBs, and TEC estimation is subject to data pre-processing which includes cycle slips removal/correction in the carrier-phase data, outlier detection and removal if any, levelling of phase-derived TEC to code-derived TEC, least squares fitting of ionosphere model (e.g., 15^{th} order spherical harmonic) to the data etc. Since we have not used the same GNSS processing tool and historical data (i.e., 3-day period) as the CODE, minor differences may contribute to the DCB differences we observed in Figs. 3 and 4.

Figure 5 compares the GPS satellite DCBs provided by CODE and IGS (based on ground data), and DCBs estimated from LEO only data for selected days in 2019 and 2023. Note that in case of LEO, only multi-layer MF (blind option) is used since there is no standard single-layer mapping model for LEO data.

When comparing Figs. 3 and 5, we find that the satellite DCBs computed from LEO only data do better match (i.e., right panel is showing less DCB differences in Fig. 5) with the CODE product compared to the DCBs obtained from the ground only data (see Fig. 3). All four plots in right panel of Fig. 5 show that the red bars are smaller than the green bars indicating less

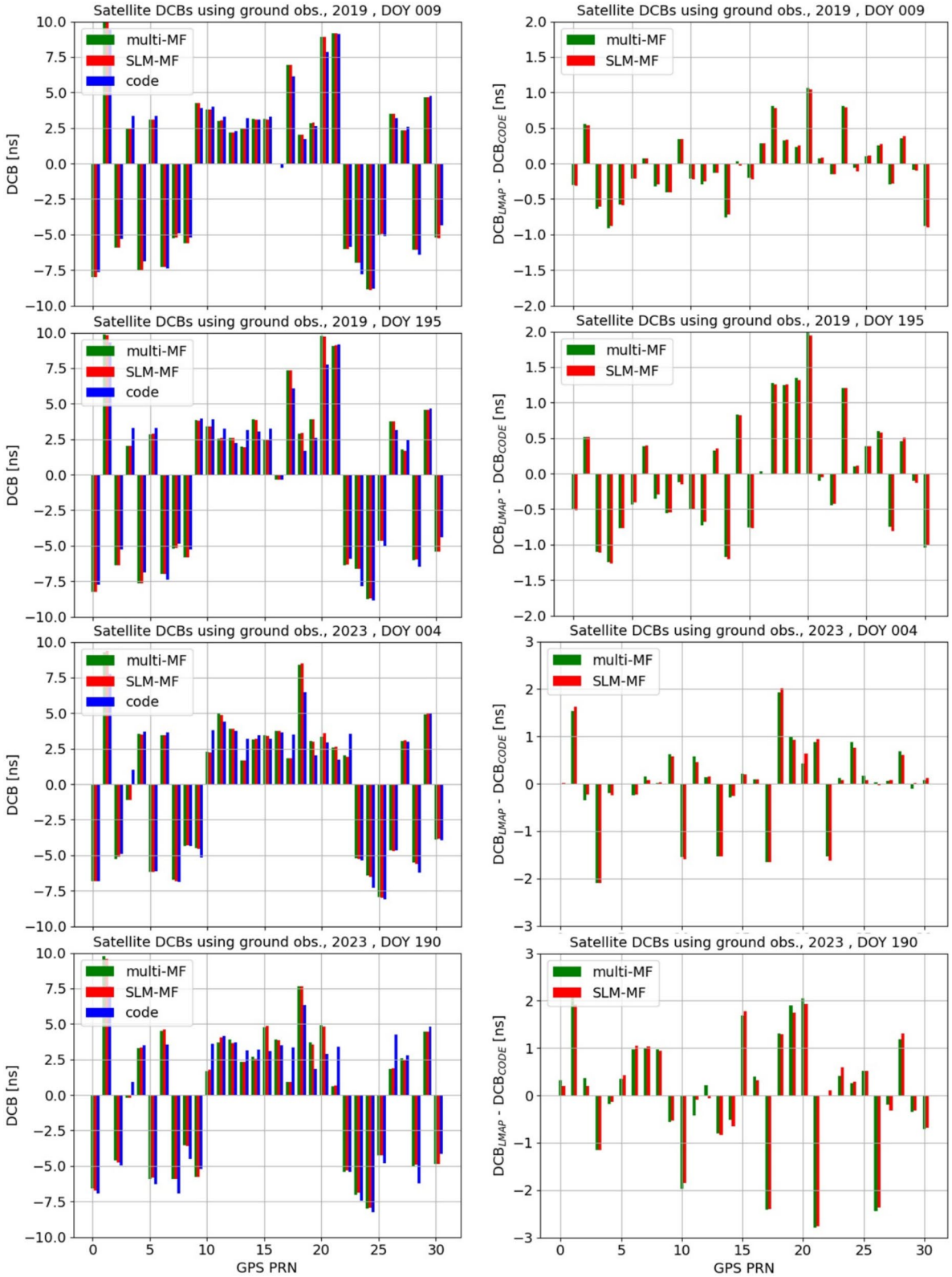

Fig. 3 GPS satellite DCBs estimated from ground observations. Left panel: blue bar shows reference DCBs provided by CODE, and green and red bars show DCBs computed using multi-layer and single-layer MF. Right panel: green (multi-layer MF) and red bars show the differences between CODE DCBs and LMAP estimation. The year and Day of Year (DOY) are given in figure title

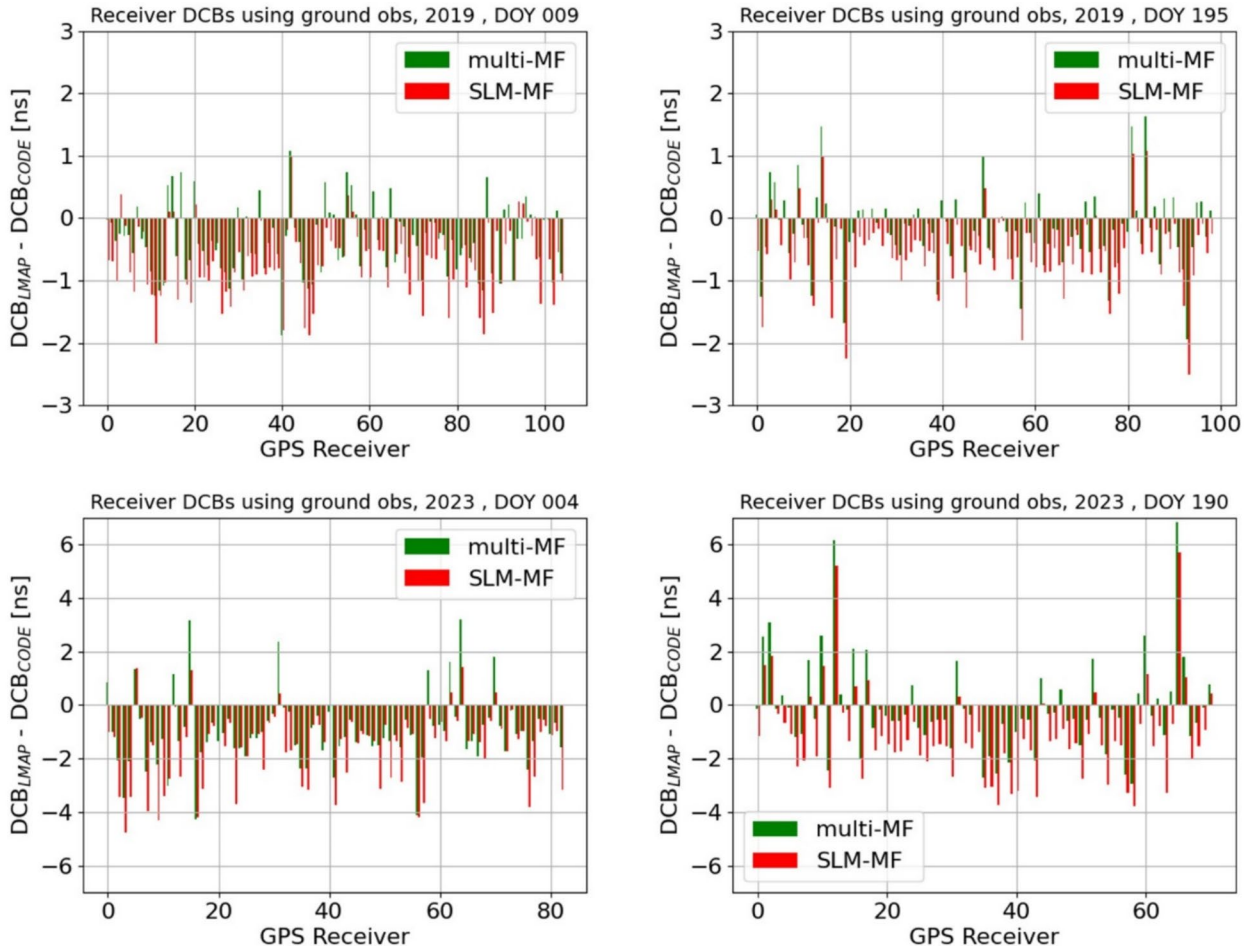

Fig. 4 In each plots the green (multi-layer MF) and red (single-layer MF) bars show the differences between CODE and LMAP computation of ground receiver DCBs

errors for LMAP products when comparing with IGS combined products. We found up to 0.1 and 0.5 ns less error during 2019 and 2023, respectively, for LMAP products when comparing satellite DCBs with IGS combined products instead of CODE products. Therefore, LEO data are able to compute GNSS satellite DCBs accurately. The plots for the 2nd day in each Test Cases (e.g., 10th Jan & 15th Jul 2019, 15th Jan & 10th Jul 2023) are very similar to the first day plots and therefore, they are not included here.

The global distribution of receiver DCB differences (absolute values) between CODE and LMAP results is given for the 9th & 14th July 2019 and 4th & 10th July 2023 in Fig. 6.

In Fig. 6, the bigger the size of the circle the bigger the errors. The smaller circle for low solar activity year 2019 indicates less DCB errors for both MFs (see left panel). Most cases the blue circles encircle the red circles indicating less error or better performance for the multi-layer MF approach. We found that the multi-layer MF gives less errors over Europe, North America, North Africa and Asia. The bigger spheres are found mainly at low latitude regions and close to oceans where data coverage is sparse. The shaded ellipsoids indicate the geolocation of receivers for which the multi-layer MF performs worse than the single-layer MF. As shown in left panel of Fig. 6, such areas are identified over the South America, South Africa and high latitude regions during low solar activity condition. During high solar activity conditions (see right panel), such receivers are distributed over the South America, South Africa and South Atlantic regions. Since the receivers are distributed over a large region in the Southern hemisphere, we assume that the blind TEC model used (i.e., NTCM) in multi-layer MF may be not performing well over the Southern hemisphere. The NTCM model was derived from the GNSS TEC data

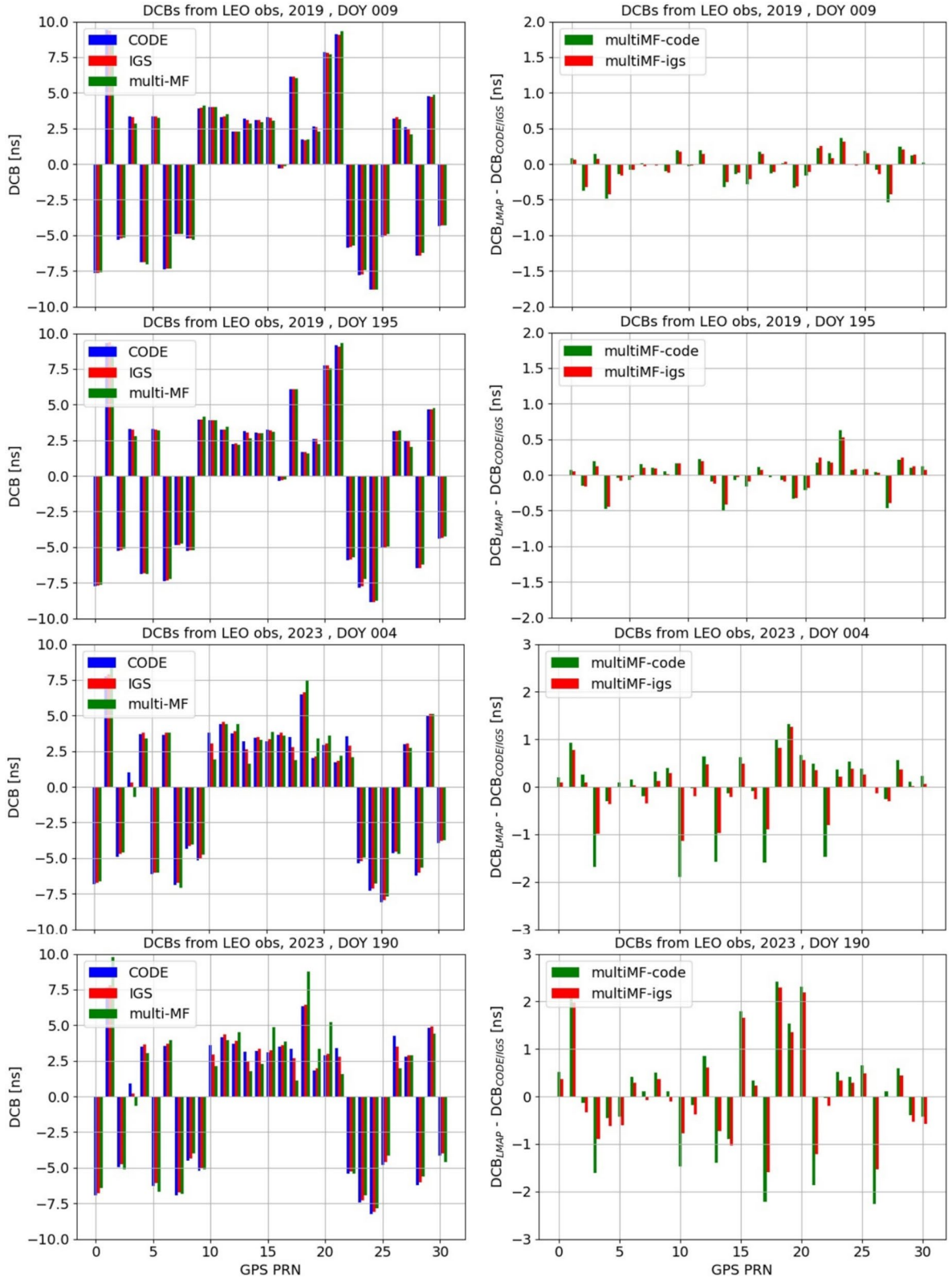

Fig. 5 GPS satellite DCBs estimated from LEO only observations (LMAP product). Left panel: blue and red bars show reference DCBs from CODE and IGS combined products, and green bar shows DCBs computed using multi-layer MF in our analysis. Right panel: green and red bars show the differences between CODE & LMAP and IGS & LMAP products, respectively

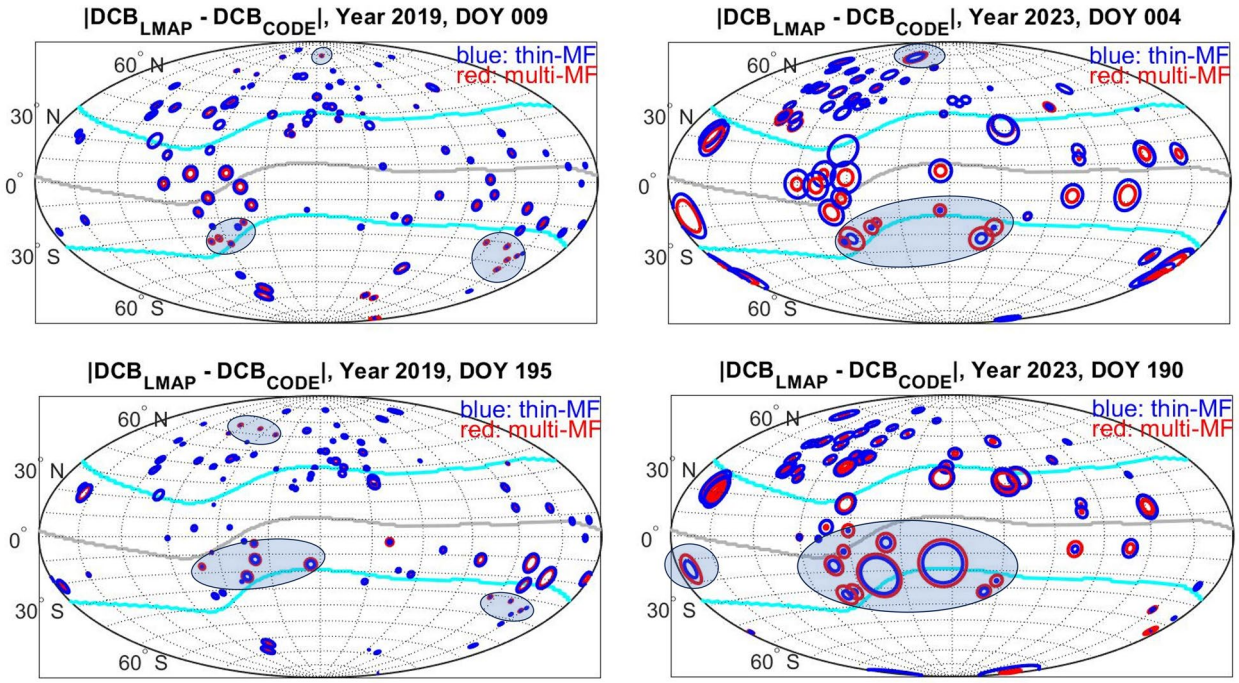

Fig. 6 Global distribution of receiver DCB differences (absolute values) between CODE and our computation on 9th Jan & 14th July 2019 (left panel) and 4th Jan &10th Jul 2023 (right panel). The blue and red circles show the error for the single-layer and multi-layer MF, respectively. The shaded ellipsoid indicates the region where the single-layer MF outperforms the multi-layer MF

during 1998–2007 and the station distribution over the Southern hemisphere was sparse. Also, the assumption of fixed peak density hmF2 height (e.g., 350 km) and fixed scale height (e.g., 70 km) may deviate significantly from the actual values especially during perturbed geomagnetic and high solar activity conditions. Use of improved TEC model and key ionospheric parameters may improve the multi-layer MF performance.

LEO receiver DCBs

In this section, we compared the computed LEO receiver DCBs with reference/legacy data products from UCAR and ESA. Table 1 gives the LEO receiver DCBs computed for selected days.

Table 1 shows that the LEO receiver DCBs between UCAR and LMAP products differ up to 3 TECU where 1 TECU = 10^{16} el/m^2. In general, this is the accuracy level of the COSMIC-1 DCB products as reported by UCAR (see Yue et al., 2011). The LEO receiver DCBs for Swarm (-A, -B and -C satellites) are found within the 1–3 TECU range when comparing with ESA's Swarm data products. According to Zhou et al. (2020) the nominal errors of the DCBs given in the Swarm Level 2 products are about 0.5 ns (or 1.42 TECU).

Similarly, the LEO receiver DCBs for MetOp (-A, -B and -C satellites) are found within the 1–3 TECU range when comparing with UCAR data products. The computed LEO receiver DCBs for COSMIC-2 (six satellites) mission are found to differ largely up to 5–10 TECU and even more when comparing with the UCAR data products. However, Pedatella et al. (2021) reported that the accuracy of the COSMIC-2 TEC observations is within 3.0 TECU. We found that the used RINEX data had many discontinuous data arcs and therefore, the preprocessing could not remove the outliers in many cases which might influence our DCB estimation.

The LEO receiver DCBs for the 2nd day in each Test cases (e.g., 10th Jan & 15th Jul 2019, 15th Jan & 10th Jul 2023) are very similar to the first day values and therefore, they are not included in Table 1.

Comparison with CODE and IGS GIMs

We compared LMAP reconstructed GIMs with reference GIMs from CODE and IGS in terms of daily histograms of TEC differences. We obtained very similar results for CODE and IGS combined data products and therefore, to avoid redundancy, we only provided relevant plots for comparison with CODE products (see Fig. 7). However, the discussion includes results from both comparisons. The available CODE/IGS GIMs have one/two-hour time resolution. Therefore, the vertical TEC differences ($TEC_{LMAP} - TEC_{CODE}$ and $TEC_{LMAP} - TEC_{IGS}$) are computed every one/two hour interval at each latitude/longitude grid points. The TEC differences are separately

computed for two types- GIM with multi-layer MF and GIM with single-layer MF. From those TEC differences daily histogram plots are derived for both products. The statistical estimates such as the root mean square (rms), mean and standard deviations (std) of TEC differences are computed and given in each histogram plot for both MF types. Green and red coloured plots in Fig. 7 represent the results for multi-layer and single-layer mapping function, respectively. Comparing rms, mean and std values in left panel, we see that the LMAP GIM with multi-layer MF performs better on selected 4 days in 2019. All three statistical parameters are smaller (or equal) for the multi-layer MF GIM. We have found that the rms and std lie within 2 TECU for LMAP multi-layer MF products and the mean deviation is below 0.5 TECU. In case of LMAP single-layer MF products, the rms and mean lie slightly above 2 TECU and mean is about 1 TECU.

Comparing the rms, mean and std values given in the right panel of Fig. 7, we see that the LMAP GIM with multi-layer MF performs better in terms of mean deviation on selected 4 days in 2023. The mean deviation is approximately -1.5 TECU for multi-layer MF GIM and around -4 TECU for single-layer MF GIM for 4^{th} and 15^{th} Jan 2023. The rms deviation is approximately same as about 8/9 TECU for both MFs. However, the std is about 1 TECU less for the single-layer MF case. We compared LMAP GIMs with CODE as well as with IGS combined GIMs. The rms, mean and std of TEC differences ($TECL_{MAP} - TEC_{CODE\ /\ IGS}$) are averaged for each group of days in Table 2.

We found that regardless of the selection of the benchmark, either CODE or IGS, the rms and mean deviations are less for the multi-layer MF. For both MFs, the mean deviations are much less for the low solar activity year 2019 compared to the high solar activity year 2023. Northern Summer days in July have less mean bias compared to winter days during both years. The perturbed geomagnetic and high solar activity days (4^{th} & 15^{th} Jan 2023) have the largest mean bias about −4.8 and −2.2 TECU for both MFs. The rms and std values are about 2–4 times higher during the perturbed-geomagnetic and high solar activity conditions compared to the quiet-geomagnetic and low solar activity conditions. As already mentioned, ionosphere is more dynamic during perturbed and high solar activity conditions and difficult to model; therefore, we obtained higher TEC differences for LMAP GIMs regardless of the choice of the benchmark. Figure 4 shows that the receiver DCB differences between LMAP and CODE products are about 3 ns for many stations and some cases up to 6 ns during 2023. Again Fig. 3 shows that the satellite DCB differences between LMAP and CODE products can be over 2 ns during perturbed and high solar conditions. The quantity 1 ns DCB leads to ~ 2.9 TECU when determining GPS L1-L2 dual-frequency TEC. Therefore, the larger TEC differences between the LMAP and CODE/IGS GIMs during the perturbed and high solar conditions come from the larger differences in the satellite and receiver DCBs. To analyse how the results vary across different latitudinal regions we divided geographic latitude into three regions: a low latitude region between 30° S and 30° N, middle latitude regions between 60–30° S and 30–60° N and high latitude regions between 90–60° S and 60–90° N. All longitudes are included in each region. Table 3 shows rms, mean and std of TEC differences (TEC_{LMAP}

Table 1 LEO DCBs computed using multi-layer MF approach

LEO	9^{th} Jan 2019		14^{th} Jul 2019		4^{th} Jan 2023		9^{th} Jul 2023	
	LMAP [TECU]	UCAR/ESA [TECU]	LMAP [TECU]	UCAR/ESA [TECU]	LMAP [TECU]	UCAR/ESA [TECU]	LMAP [TECU]	UCAR/ESA [TECU]
COSMIC1-C006POD2	−34.37	−31.83	−26.37					
Swarm-A	−16.42	−15.43	−16.04	−14.50	−19.53	−16.78		
Swarm-B			−8.89	−6.93	−10.49	−9.42		
Swarm-C			−13.21	−12.14	−15.49	−12.15		
MetOp-A	6.80	8.96	6.96	8.61				
MetOp-B	0.69	3.46	1.07					
MetOp-C			2.00		−2.19			
SENTINEL-3A	11.66		15.01		12.46		13.71	
SENTINEL-3B	5.70		4.45		4.47		4.02	
TSRX	−48.6		−48.05					

The corresponding DCBs provided by UCAR and ESA are written in the next column for comparison

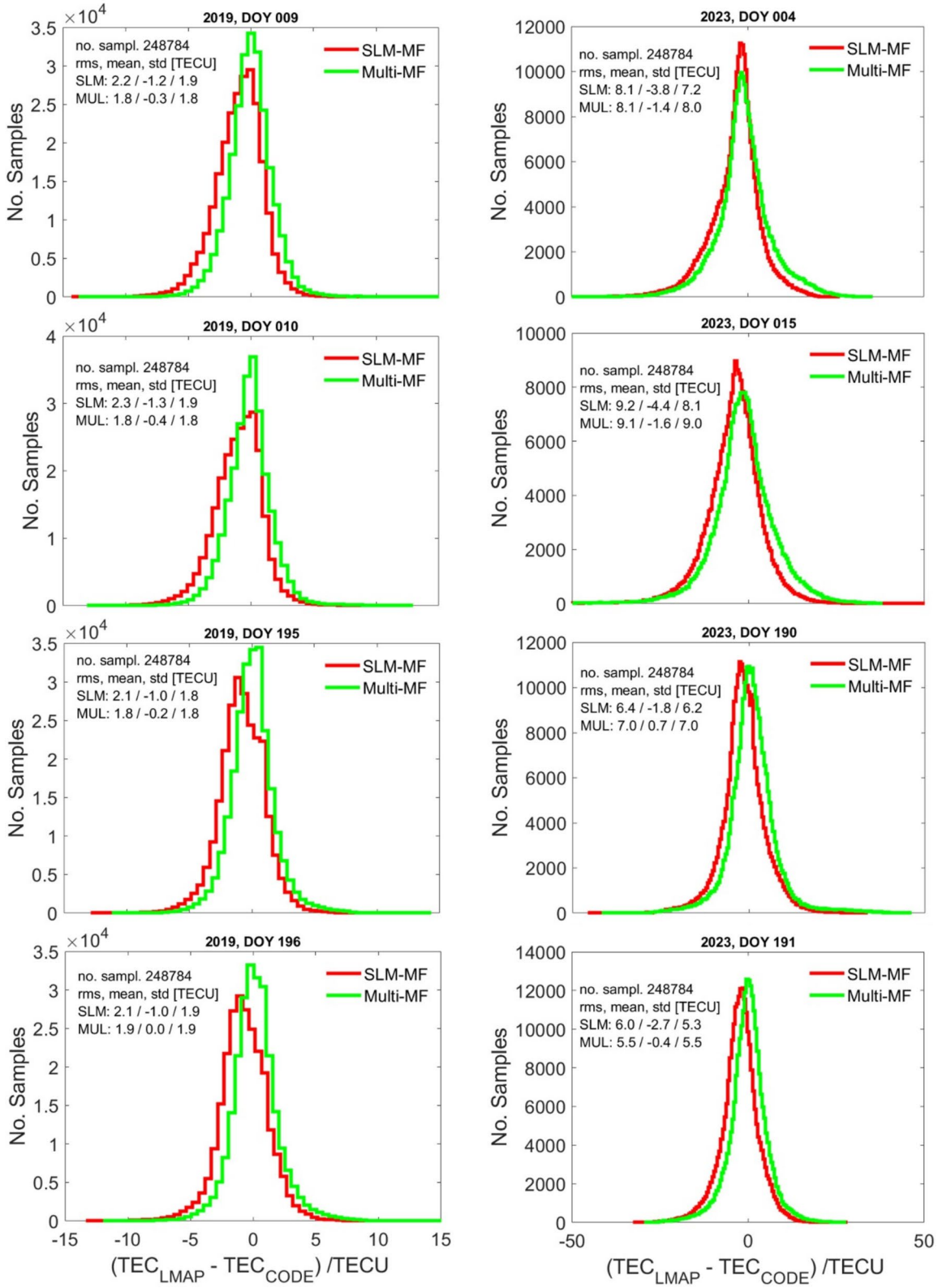

Fig. 7 Histograms of TEC differences between LMAP and CODE products for 9th Jan & 14 Jul 2019 (left panel) and 4th Jan & 9th July 2023. Red and blue coloured plots represent the results for multi-layer and single-layer mapping function, respectively

– TEC_{CODE}) for low, middle and high latitude regions separately for single-layer and multi-layer MF models for selected days in 2019 and 2023.

Table 3 shows that during 2019, in all cases, the rms and mean values are less for the multi-layer MF. The std values are up to 0.2 TECU higher for multi-layer MF in the low latitude region whereas the std values are approximately the same for both MFs in middle and high latitude regions. During 2023, in all cases, the mean values are less for the multi-layer MF. In low latitude, the rms values are less for the multi-layer MF for all days except 9th July 2023 whereas the std values are always higher (up to 1.8 TECU) for the multi-layer MF. In middle latitude, the rms and std values are less for the single-layer MF for most of the days. In high latitude, the rms values are less for the multi-layer MF for all days except 4th January 2023. The std values are found higher (up to 0.4 TECU) for the multi-layer MF during 4th & 15th January and less (up to 0.6 TECU) during 14-15th July 2023. Note that the reduction in mean deviation is consistent throughout all regions and all selected days. The reduction in mean deviation is the highest in the low latitude region showing up to 1.6 and 4.3 TECU reduction during 2019 and 2023, respectively.

Comparison with Jason-3 altimeter data

Figure 8 shows the vertical TEC comparison against Jason-3 altimeter data. Noted that the Jason-3 product represents vertical TEC for altimeter-to-ground path (below 1330 km height) whereas LMAP/CODE/IGS generated GIM product represents TEC for GNSS-to-ground path (up to 20,000 km). Therefore, both TEC products are not equivalent. Considering this, as reference, again CODE/IGS GIM data is included in the investigation. The vertical TEC values are derived for both LMAP products and CODE/IGS GIM along Jason-3 orbit (using the exact latitude and longitude location) for the selected day. The daily TEC differences are derived by subtracting the Jason-3 TECs from LMAP/CODE/IGS TECs (i.e., TEC_{LMAP} – TEC_{Jason}) at the same location. The left panel shows the histogram plots of vertical TEC differences for LMAP and CODE GIMs. We cannot distinguish which LMAP product is performing better. However, the right panel plots, where we make histogram plots of TEC differences between LMAP and CODE GIMs along the Jason orbit, show that LMAP multi-layer MF product is much closer to CODE GIM. All three statistical parameters (rms, mean and std) are smaller for the multi-layer MF GIM.

The two bottom plots in left panel show bulge like features in the histogram plots on both side of the zero-deviation line for LMAP and CODE products. One reason may be that Jason-3 captures certain ionospheric features over the oceans where there is no GNSS stations for capturing similar features by LMAP and CODE GIMs. We see similar patterns in the histogram plots on 14th and 15th Jul 2019 and no such features during 9th and 10th Jan 2019. We obtained very similar results when the IGS GIM is taken as the reference instead of the CODE GIM.

Conclusion

For the first time, we have investigated the benefit of multi-layer MF over the single-layer MF function in computing the GPS satellite and receiver DCBs, and GIMs using ground data during quiet and perturbed ionospheric conditions. We found that the choice of mapping function (either multi-layer or single layer model) hardly influences the GPS satellite DCB estimation from ground data. However, the GPS ground receiver DCB estimation improves (i.e., closer to CODE and IGS benchmark) by the use of multi-layer MF. When compared with IGS/CODE DCBs, we found that the mean receiver DCB estimation is improved by about 0.14 – 0.27 and 0.30 – 0.78 ns during days in 2019 and 2023, respectively. The maximum improvement is found to be 0.75 and 2.2 ns during 2019 and

Table 2 Statistical estimates of TEC differences between LMAP GIM and CODE/IGS GIM

In TECU	Low solar activity 2019		High solar activity 2023	
	Avg. 9–10th Jan	Avg. 14–15th Jul	Avg. 4th, 15th Jan	Avg. 9–10th Jul
	CODE / IGS	CODE / IGS	CODE / IGS	CODE / IGS
SLM: rms	2.25 / 2.90	2.10 /2.60	8.65 / 8.70	6.20 / 6.20
MUL: rms	1.80/ 2.10	1.85 / 2.00	8.60 / 8.30	6.25 / 6.00
SLM: mean	**−1.25 /− 2.10**	**−1.00 / −1.85**	**−4.10 /−4.80**	**−2.25 / −3.10**
MUL: mean	**−0.35 / −1.20**	**−0.10 / −0.95**	**−1.50 / −2.20**	**−0.55 / −0.70**
SLM: std	1.90/ 1.90	1.85 /1.85	7.65 / 7.25	5.75 / 5.40
MUL: std	1.80 / 1.75	1.85 / 1.80	8.50 / 7.95	6.25 / 5.95

Since the improvement in mean deviation using multi-layer MF is consistent throughout the Table their values are marked with bold font

Table 3 Statistical estimates of TEC differences between LMAP GIM and CODE GIM at low, middle and high latitude regions

Low solar activity 2019				
In TECU	**9th Jan**	**10th Jan**	**14th Jul**	**15th Jul**
0 < =|Lat| < = 30°	MUL/SLM	MUL/SLM	MUL/SLM	MUL/SLM
rms	2.2 / 2.9	2.2 / 2.9	2.4 / 2.7	2.5 / 2.8
mean	**−0.5 / −2.1**	**−0.6 / −2.1**	**−0.2 / −1.5**	**0.2 / −1.3**
std	2.1 / 2.0	2.1 / 2.1	2.4 / 2.2	2.5 / 2.4
30° < |Lat| < = 60°				
rms	1.8 / 2.1	1.9 / 2.3	1.5 / 1.8	1.6 / 1.9
mean	**−0.3 / −1**	**−0.5 / −1.2**	**−0.2 / −0.9**	**−0.2 / −1.0**
std	1.7 / 1.9	1.8 / 2.0	1.5 / 1.5	1.6 / 1.6
60 < |Lat| < = 90°				
rms	1.2 / 1.4	1.1 / 1.3	1.2 / 1.5	1.2 / 1.6
mean	**0 / −0.5**	**0 / 0.4**	**−0.1 / −0.5**	**0 / −0.5**
std	1.2 /1.3	1.1 / 1.2	1.2 / 1.5	1.2 / 1.5
High solar activity 2023				
	4th Jan	**15th Jan**	**9th Jul**	**10th Jul**
0 < =|Lat| < = 30°	MUL/SLM	MUL/SLM	MUL/SLM	MUL/SLM
rms	9.5 / 10.6	11.6 / 11.9	9.5 / 7.9	6.8 / 7.4
mean	**−2.9 / −7.2**	**−2.3 / −6.5**	**1.8 / −2.2**	**−0.7 / −4.3**
std	9.1 / 7.7	11.4 / 10.0	9.4 / 7.6	6.8 / 6.0
30° < |Lat| < = 60°				
rms	8.4 / 7.2	8.2 / 7.7	5.9 / 5.7	5.1 / 5.3
mean	**−0.1 / −2.2**	**−0.1 / −2.4**	**0.2 / −1.6**	**0 / −2.3**
std	8.4 / 6.9	8.2 / 7.3	5.9 / 5.4	5.1 / 4.8
60 < |Lat| < = 90°				
rms	5.7 / 5.5	6.4 / 6.7	4.4 / 5.2	4.0 / 4.6
mean	**−1.0 /−1.7**	**−2.4 / −4.1**	**−0.1 / −1.6**	**−0.4 / −1.3**
std	5.6 / 5.3	6.0 / 5.4	4.4 / 5.0	4.0 / 4.5

Since the improvement in mean deviation using multi-layer MF is consistent throughout the Table their values are marked with bold font

2023, respectively. We found that the receiver DCB estimation improves (i.e., closer to CODE and IGS benchmark) for about 68–81% and 66–87% of stations during 2019 and 2023, respectively.

Our investigation shows that the global ionosphere maps generated using multi-layer MF performs better than those using the single-layer MF for all selected days characterized by geomagnetic and solar conditions. The statistical parameters such as the root mean square, mean and standard deviations of TEC differences between generated GIMs and CODE/IGS products show smaller values for the multi-layer GIM indicating better performance. The mean bias/deviation is about 0.8–1 TECU and 1.1–2.8 TECU less for the multi-layer MF during low and high solar activity year 2019 and 2023, respectively. When comparing with Jason-3 altimeter data we found that the statistical parameters such as the root mean square, mean and standard deviations of TEC differences are closer to those of IGS/CODE GIMs for the multi-layer MF indicating better performance.

In addition, multi-missions LEO data have been combined using multi-layer MF approach, and the GPS satellite and LEO receiver DCBs are computed. The LEO only data gives better results than ground only data when comparing satellite DCBs against the reference/legacy DCBs from IGS/CODE. This indicates that the LEO only data are able to compute GNSS satellite DCBs accurately. The accuracy of computed LEO receiver DCBs is found about 1–3 TECU for COSMIC-1, Swarm and MetOp missions which is within the accuracy level of the UCAR and Swarm data products.

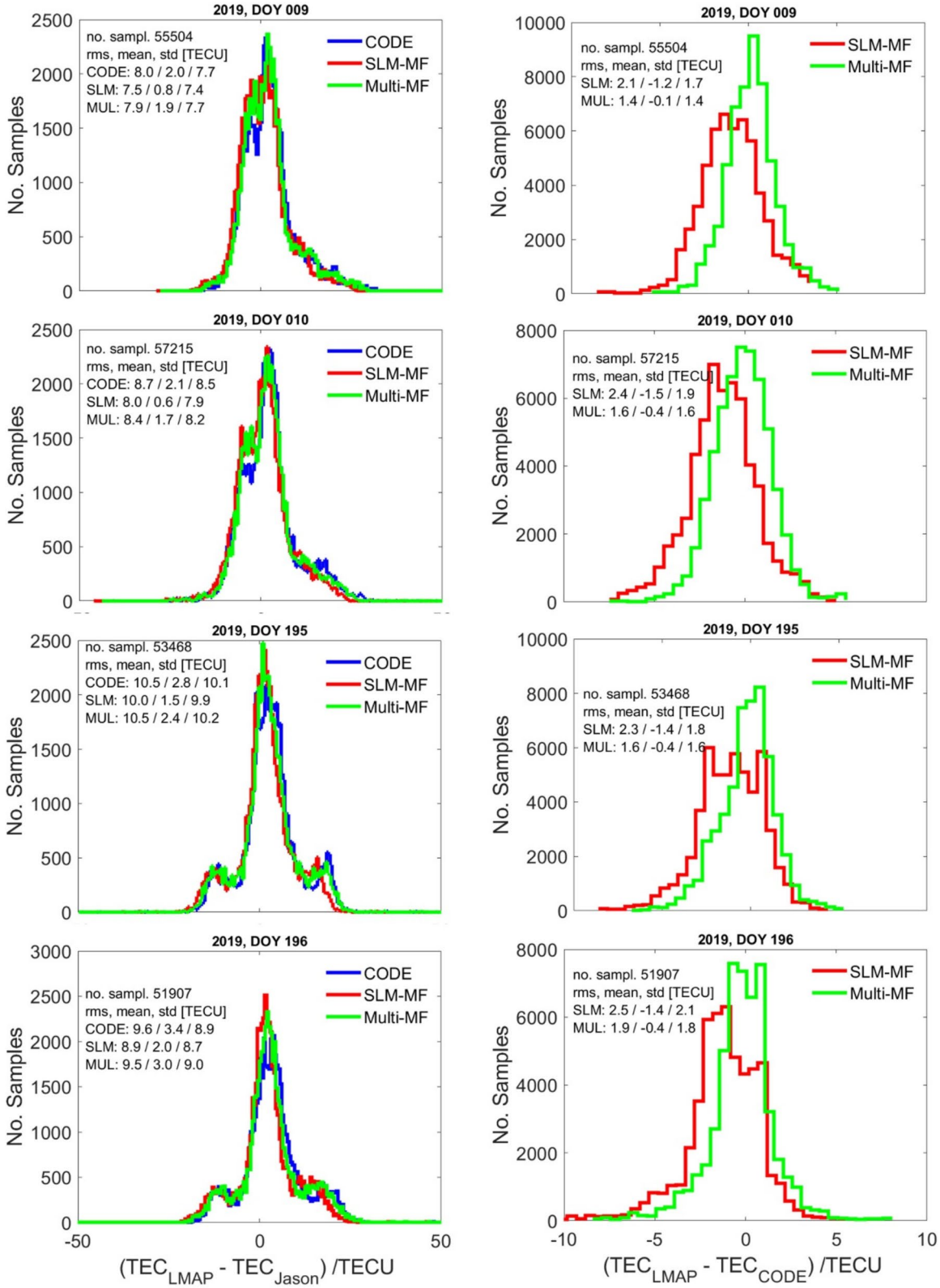

Fig. 8 Histogram of TEC differences between LMAP and Jason-3 products. Left panel: the green and red coloured plots represent the results for LMAP products with multi-layer and single-layer MF, respectively, and the blue plot represents CODE GIM results. Right panel: the green and red plots represent the TEC deviation from CODE GIM values along Jason-3 orbit, for LMAP multi-layer MF and single-layer MF products, respectively

Acknowledgement
The authors give thanks to sponsors and operators of NASA's Earth Science Data Systems and the CDDIS for archiving and distributing GNSS data and GIMs from IGS and making available GNSS data onboard Sentinel satellites. The authors are grateful to the University Corporation for Atmospheric Research (UCAR) for processing and making available GNSS data onboard COSMIC-1, COSMIC-2, MetOp and TerraSAR-X satellites. The authors give thanks to ESA for making available GPS data onboard Swarm satellites. The authors give thanks to DGFI-TUM for processing Jason-3 altimeter data and making available via Open Altimeter Database.

Author contributions
Conceptualization- M.M. Hoque, L. Yuan; methodology- M.M. Hoque, L Yuan, G Nykiel.; software- L. Yuan, M.M. Hoque, G Nykiel, O. Frauenberger, N. Dhital; formal analysis- J Paziewski, R. Sieradzki; writing—original draft preparation – MM Hoque; writing—review and editing- G. Nykiel, L. Yuan, P. Wielgosz; funding acquisition- R. Orus, M.M. Hoque.

Funding
The work is partly funded by the LMAP (LEO Ionospheric Mapping Assessment and Derivation For Precise PVT Applications) project under the ESA Contract No. 4000142821/23/NL/MGu/my.

Availability of data and materials
The database used and links to the data sources are given explicitly for each data types in the Sect. 3 namely "Database and data processing".

Declarations

Competing interests
Mohammed Mainul Hoque is an editorial board member for Satellite Navigation and was not involved in the editorial review or decision to publish this article. The authors declare no competing interests. The funders had no role in the design of the study; in the collection, analyses, or interpretation of data; in the writing of the manuscript, or in the decision to publish the results.

Received: 25 July 2025 Revised: 6 November 2025 Accepted: 11 November 2025
Published online: 15 December 2025

References

Berdermann, J., Jakowski, N., Hoque, M.M., HIubek, N., Missling, K.D., Kriegel, M., Borries, C., Wilken, V., Barkmann, H. & Tegler, M. (2014). Ionospheric monitoring and prediction center (IMPC). *Proceedings of the 27th International Technical Meeting of the Satellite Division of The Institute of Navigation (ION GNSS+ 2014)*, Tampa, Florida, pp. 14–21.

Bilitza, D. (2001). International reference ionosphere 2000. *Radio Science, 36*, 261–275. https://doi.org/10.1029/2000RS002432

Chapman, S. (1931). The absorption and dissociative or ionizing effect of monochromatic radiation in an atmosphere on a rotating earth part II. Grazing incidence. *Proceedings of the Physical Society (Great Britain)*. https://doi.org/10.1088/0959-5309/43/5/302

Foelsche, U., & Kirchengast, G. (2002). A simple "geometric" mapping function for the hydrostatic delay at radio frequencies and assessment of its perfor-mance. *Geophysics Research Letters*, *29*(10), Article 111. https://doi.org/10.1029/2001GL013744

Gallagher, D. L., Craven, P. D., & Comfort, R. H. (2000). Global core plasma model. *Journal of Geophysical Research, 105*, 18819–18833. https://doi.org/10.1029/1999JA000241

Hoque, M. M., & Jakowski, N. (2007). Mitigation of higher order ionospheric effects on GNSS users in Europe. *GPS Solutions*,*12*, 87–97.https://doi.org/10.1007/s10291-007-0069-5

Hoque, M. M., & Jakowski, N. (2011). A new global empirical NmF2 model for operational use in radio systems. *Radio Science*, *46* (6), 1–13. https://doi.org/10.1029/2011RS004807

Hoque, M. M., & Jakowski, N. (2012). A new global model for the ionospheric F2 peak height for radio wave propagation. *Annales Geophysicae, 30*, 797–809. https://doi.org/10.5194/angeo-30-797-2012

Hoque, M. M., Yuan, L., Prol, F. S., Hernández-Pajares, M., Notarpietro, R., & Marquardt, C. (2023). A new method of electron density retrieval from MetOp-A's truncated radio occultation measurements. *Remote Sensing, 15*, Article 1424. https://doi.org/10.3390/rs15051424

Hoque, M.M. & Jakowski, N. (2013), Mitigation of ionospheric mapping function error. *Proceedings of the 26th International Technical Meeting of the Satellite Di-vision of The Institute of Navigation (ION GNSS+ 2013)*. Nashville, TN, pp. 1848–1855.

Hoque, M.M., Jakowski, N. & Berdermann, J. (2014). A new approach for mitigating ionospheric mapping function errors. *Proceedings of the 27th International Technical Meeting of the Satellite Division of The Institute of Navigation (ION GNSS+ 2014)*. Tampa, Florida, pp. 1183–1189.

Huo, X., Long, Y., Liu, H., Yuan, Y., Liu, Q., Li, Y., & Sun, W. (2024). A novel ionospheric TEC mapping function with azimuth parameters and its application to the Chinese region. *Journal of Geodesy, 98*(2), 13.

Jakowski, N. (2005). Ionospheric GPS radio occultation measurements on board CHAMP. *GPS Solutions, 9*, 88–95. https://doi.org/10.1007/s10291-005-0137-7

Jakowski, N., & Hoque, M. M. (2018). A new electron density model of the plasmasphere for operational applications and services. *Journal of Space Weather and Space Climate, 8*, A16. https://doi.org/10.1051/swsc/2018002

Jakowski, N., & Hoque, M. M. (2021). Global equivalent slab thickness model of the Earth's ionosphere. *Journal of Space Weather and Space Climate, 11*, 10. https://doi.org/10.1051/swsc/2020083

Jakowski, N., Hoque, M. M., & Mayer, C. (2011a). A new global TEC model for estimating transionospheric radio wave propagation errors. *Journal of Geodesy, 85*(12), 965–974. https://doi.org/10.1007/s00190-011-0455-1

Jakowski, N., Mayer, C., Hoque, M. M., & Wilken, V. (2011b). TEC models and their use in ionosphere monitoring. *Radio Science, 46*, Article RS0D18. https://doi.org/10.1029/2010RS004620

Lear, W.M. (1988). GPS navigation for low earth orbiting vehicles. *NASA 87-FM-2, Rev. 1, JSC-32031, Lyndon B.* Johnson Space Center, Mission planning and analysis division.

Pedatella, N. M., Zakharenkova, I., Braun, J. J., Cherniak, I., Hunt, D., Schreiner, W. S., & Wu, Q. (2021). Processing and validation of FORMOSAT-7/COSMIC-2 GPS total electron content observations. *Radio Science, 56*(8), 1–15. https://doi.org/10.1029/2021RS007267

Rishbeth, H., & Garriott, O. K. (1969). *Introduction to ionospheric physics*. Academic Press.

Schaer, S., Beutler, G. & Rothacher, M. (1998). Mapping and predicting the ionosphere. In: Dow JM, Kouba J, Springer T (Eds.), *Proceedings of the 1998 IGS analysis center workshop*, Darmstadt, pp. 307–318.

Wang, Y. (2003). A numerical study on the difference of several definitions of shell height in thin-shell model. *J Jingzhou Teach Coll (Nat Sci), 26*, 35–38.

Wang, N., Li, Z., Duan, B., Hugentobler, U., & Wang, L. (2020). GPS and GLONASS observable-specific code bias estimation: comparison of solutions from the IGS and MGEX networks. *Journal of Geodesy*, 94, 74. https://doi.org/10.1007/s00190-020-01404-5

Xiang, Y., & Gao, Y. (2019). An enhanced mapping function with ionospheric varying height. *Remote Sensing, 11*(12), Article 1497. https://doi.org/10.3390/rs11121497

Yuan, L., Jin, S., & Hoque, M. (2020). Estimation of LEO-GPS receiver differential code bias based on inequality constrained least square and multi-layer mapping function. *GPS Solutions, 24*, Article 57. https://doi.org/10.1007/s10291-020-0970-8

Yuan, L., Hoque, M., & Jin, S. (2021). A new method to estimate GPS satellite and receiver differential code biases using a network of LEO satellites. *GPS Solutions, 25*, Article 71. https://doi.org/10.1007/s10291-021-01109-y

Yue, X., Schreiner, W.S., Rocken, C. & Kuo, Y.H. (2011). Evaluation of the LEO based slant TEC data. *5th FORMOSAT-3/COSMIC Data Users Workshop,* Taipei, Taiwan.

Zhong, J., Lei, J., Dou, X., & Yue, X. (2016). Assessment of vertical TEC mapping functions for space-based GNSS observations. *GPS Solutions, 20*(3), 353–362.

Zhou, P., Nie, Z., Xiang, Y., Wang, J., Du, L., & Gao, Y. (2020). Differential code bias estimation based on uncombined PPP with LEO onboard GPS observations. *Advances in Space Research, 65*(1), 541–551.

Publisher's Note